

# Back-illuminated Si-based photoanode with nickel cobalt oxide catalytic protection layer

**Bae, Dowon; Mei, Bastian Timo; Frydendal, Rasmus; Pedersen, Thomas; Seger, Brian; Hansen, Ole; Vesborg, Peter Christian Kjærgaard; Chorkendorff, Ib**

*Published in:*
ChemElectroChem

*Link to article, DOI:*
10.1002/celc.201500554

*Publication date:*
2016

*Document Version*
Peer reviewed version

# Back-illuminated Si based photoanode with nickel cobalt oxide catalytic protection layer

Dowon Bae,[a] Bastian Mei,[a] Rasmus Frydendal,[a] Thomas Pedersen,[b] Brian Seger,[a] Ole Hansen,[a,b] Peter C. K. Vesborg[a] and Ib Chorkendorff*[a]

**Abstract:** Si is an excellent photoabsorber for use in dual band gap photoelectrochemical water splitting. We investigate photoanodes with $n^+pp^+$-Si configuration under back-side illumination which is suited to work in a tandem device stack. A co-sputtered $NiCoO_x$ film coupled to the Si was used as a protective catalyst for the water oxidation reaction in 1M KOH. The sample showed high photocurrent (21 mA $cm^{-2}$) under the red-light (38.6 mW $cm^{-2}$). Long-term stability test showed gradual decrease of activity in the beginning, and then the activity was increased, yielding a cathodic shift of the onset voltage (> 50 mV) likely due to divergent response of Ni and Co to Fe present in KOH. Once the activity of the sample is stabilized, no further degradation was observed for the following 6 days, indicating that the demonstrated back-illuminated photoanode configuration can be considered as a promising architecture to be applied as a bottom cell of the tandem water splitting device under alkaline conditions.

## Introduction

For efficient hydrogen ($H_2$) production via water splitting reaction, both hydrogen evolution reaction (HER) and oxygen evolution reaction (OER) need to proceed with a high-rate.[1,2] However, the kinetically slow OER process has been a major bottleneck,[3] since it comprises several intermediate steps with high activation energy barriers and thus requires a high overpotential ($\eta$) to transfer the 4 electrons: $2H_2O \rightarrow 4H^+ + O_2 + 4e^-$ (in acid) or $4OH^- \rightarrow 2H_2O + O_2 + 4e^-$ (in alkaline). To overcome this problem, efficient OER catalysts are required, but the state of the art electrocatalysts for OER, such as $IrO_2$ and $RuO_2$,[4-6] are precious metal oxides and too expensive to scale-up, despite of their excellent OER activity in acidic media. In this context, earth-abundant transition metal oxides have been intensively investigated to develop cost-effective alternative OER materials with high activity.[7,8] As one of the non-noble catalyst for OER, nickel cobalt oxide (hereinafter $NiCoO_x$) has recently attracted considerable attention, despite the fact that it is stable only in alkaline media, mainly because of its excellent electrical conductivity and rich redox kinetics due to the large number of active sites.[9] Compared to elemental oxides, such as NiO and $Co_3O_4$, $NiCoO_x$ is promising candidate for applications, such as electrocatalytic anodic oxygen evolution, supercapacitors, sensors, or optical limiters and switches.[9-12] Similarly in recent studies[13,14] Fe modified NiO compounds have been demonstrated to be efficient OER catalysts. The Boettcher's group[14] found that Fe enhances the film conductivity of nickel-based oxide, and claimed that incorporated Fe enhances the OER activity through a Ni-Fe partial charge transfer activation process, as has been proposed by Corrigan et al.[15] Furthermore, this study also reported that the overpotential of $Ni(OH)_2$ film for OER can be reduced during cyclic voltammetry (CV) process in 1M KOH due to incorporation of trace amounts of Fe present in KOH.[13] Thus, unintentional, but beneficial Fe alloying or doping occurs. So far, a number of approaches to obtain functional Ni-Fe-O compounds have been reported.[13-16] Large-scale combinational screening studies[17,18] have shown that not only Ni with Fe, but also other metallic elements (e.g., Co, Al, Ce) appear to enhance the OER-activity of Ni based oxides. These recent studies indicate that various combinations of cations provide the possibility to change the electrochemical properties. At the same time, it also implies that the OER activity of $NiCoO_x$ would be also enhanced simply by aging in the electrolyte without any intentional doping procedure.

To date, many research groups have demonstrated catalytic behavior of element nickel or cobalt oxides[16,19-24] while a relatively small number of studies report the electrocatalytic activity of the binary nickel-cobalt oxides.[9-11] In the present work we demonstrate the time-dependant behavior of the OER kinetics of $NiCoO_x$ thin films in 1M KOH (pH = 14) electrolyte. The $NiCoO_x$ with Co interlayer is deposited by DC-sputtering on $p^+pn^+$ Si photoelectrodes, and we evaluate the OER kinetic variation of the sample as a function of the operating time under back side illumination. According to the Pourbaix diagrams, both nickel and cobalt oxide can be converted to hydroxides during potential cycling in alkaline electrolyte,[25,26] and both materials have been used as a protection layer of Si photoabsorbers with frontal illumination.[16,19,22,23] However, in actual tandem device operation conditions a low band gap absorber, such as Si, should be used as bottom cell of the tandem water splitting device, where the light is incident from the "dry"

[a] Dr. D. Bae, Dr. B. Mei, Dr. R. Fryndendal, Prof. B. Seger, Prof. O. Hansen, Prof. P.C.K. Vesborg, Prof. I. Chorkendorff
Center for Individual Nanoparticle Functionality
Department of Physics / Technical University of Denmark
Fysikvej B311, DK-2800 Kongens Lyngby (Denmark)
E-mail: ibchork@fysik.dtu.dk
[b] Dr. T. Pedersen, Prof. O. Hansen
Department of Micro- and Nanotechnology
Technical University of Denmark
Ørsteds Plads B344, DK-2800 Kongens Lyngby (Denmark)

Supporting information for this article is given via a link at the end of the document.

side of the photoanode. We have demonstrated successful hydrogen production using a light-permeable ring-shaped Al back contact under back-illumination condition,[27] and this approach is also employed in this study to allow illumination from the side opposing the solid/liquid interface (i.e. $NiCoO_x$ side). Since the photons are irradiated from the back contact side, transparency of the protection layer is not a required property, indicating that thick, non-transparent protection layers can be employed.

## Results and Discussion

The p-type c-Si with a shallow $n^+p$-junction at the side opposing the solid/liquid interface was coupled with a 50-nm-thick $NiCoO_x$ protective OER catalyst. The $NiCoO_x$ was deposited by co-sputtering of Ni and Co with same deposition rate (i.e. Ni:Co ≈ 1:1) under oxygen flow. The back side of the samples was covered with a quartz glass to protect back side from direct contact with the electrolyte as shown in Figure 1a. The Co interlayer was introduced to prevent oxidation of the Si surface during the metal oxide deposition, and to provide an efficient pathway for the carrier injection by forming an Ohmic contact as shown in energy band diagram (Figure 1b).

Scanning electron microscopy (SEM) images of the $NiCoO_x$ with Co interlayer deposited on a Si substrate are shown in Figure 2. Figure 2a and b correspond to cross-sectional and top-view image of the film, respectively. The cross-sectional SEM image indicates that the $NiCoO_x$ film is continuous above the Si substrate and has a thickness of about 50 nm, and thus the surface is covered completely. This also can be found from the top-view SEM image (Figure 2b) exposing a dense $NiCoO_x$ surface without any obvious cracks or pin-holes. Note that the investigated films were deposited on the Si photoelectrodes using the same conditions as those used for the PEC samples, and the presence of nickel and cobalt in the binary oxide layer

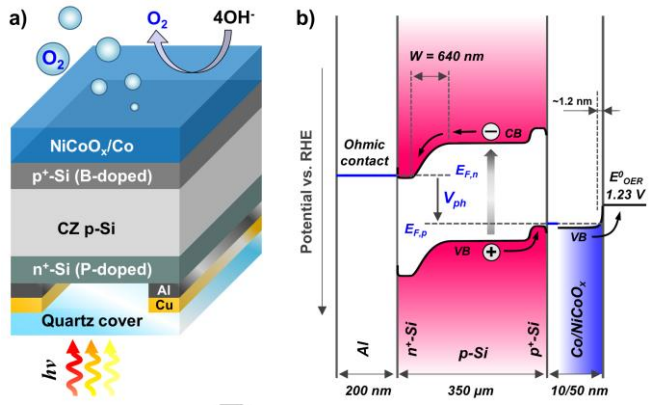


**Figure 1.** (a) Schematic drawing of the back illuminated photoanode with Al/$n^+pp^+$-Si/Co/$NiCoO_x$ ($NiCoO_x$ on top) and (b) band alignment under illumination. Energy diagram calculation procedure can be found in Supporting Information.

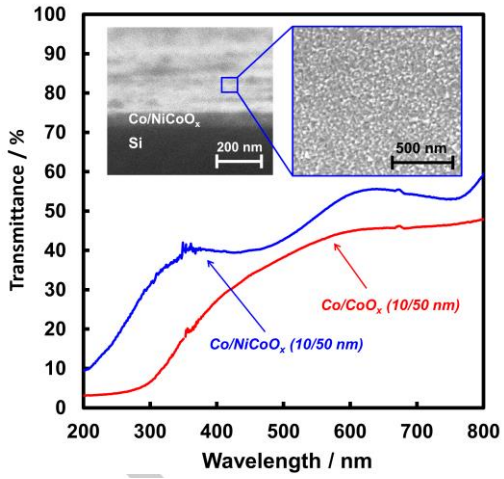


**Figure 2.** UV-Vis transmittance spectra of $NiCoO_x$ (blue) and $CoO_x$ (red) deposited on quartz substrate with Co interlayer. The signal from the quartz substrate was substracted as a background spectrum. Cross-sectional SEM image of $n^+pp^+$Si/Co/$NiCoO_x$ and top-view SEM image are also shown as inset. The $NiCoO_x$ film was deposited at 300°C, and these SEM images well demonstrate excellent surface coverage without any obvious cracks or pinholes.

was confirmed by energy dispersive X-ray spectroscopy (EDX) analysis (Figure S1 in Supporting Information). The optical behavior of the deposited films was investigated by UV-Vis transmittance spectroscopy as shown in Figure 2. Transmittance of deposited $NiCoO_x$ was only approximately 53% at 600 nm in wavelength in spite of its wide band-gap over 2.75 eV.[28] As shown in our recent work[15] a NiO thin film with 50 nm thickness shows over 80% transmittance at 600 nm wavelength due to its high band gap (3.5 ~ 3.6 eV), and thus the optical loss of $Co/NiCoO_x$ would partially due to the Co interlayer. However, a $Co/CoO_x$ layer with same thickness shows transmittance of 43% at the same wavelength having a band-gap of around 1.96 ~ 2.36 eV,[29] and it is suggested that the optical loss and decreased band gap of $NiCoO_x$ can be mainly attributed to the mixed cobalt oxide phase which shows a drastic increase of absorption coefficient with increased growth temperature.[30] This illustrates how back illumination is beneficial for photoanodes based on such overlayers.

$NiCoO_x$ is a well-known p-type, mixed-valence oxide with Ni occupying octahedral sites and Co distributed over both octahedral and tetrahedral sites.[31] To confirm the conductivity type of the present $NiCoO_x$ thin film, electrochemical impedance measurements were performed (i.e. Mott-Schottky analysis). The resulting Mott−Schottky plot (Figure S2) shows a negative slope, confirming the p-type behavior of the deposited $NiCoO_x$ films. The flat band potential ($E_{FB}$) and the acceptor density ($N_A$) were estimated to be $E_{FB} \approx 0.7$ V versus RHE and $N_A \approx 7 \cdot 10^{18}$ $cm^{-3}$, respectively, and this high dopant density should provide sufficient conductivity to transport holes through the valence band.

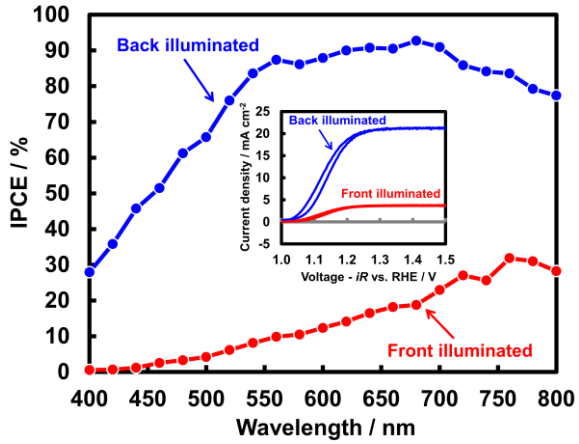


**Figure 3.** IPCE measurement results under front and back-illumination using $n^+pp^+$Si/Co/$NiCoO_x$ photoanode sample, and the inset is cyclic voltammetry scans under front and back side illumination (AM 1.5G and 635 nm cut-off filters were used in the cyclic voltammetry scans). Note that imperfect active-area definition by epoxy encased electrodes can cause a overrating of IPCE.

To verify the photoelectrochemical properties of $NiCoO_x$, this film was coupled with the $n^+pp^+$-Si photoanode with a Co interlayer between the $p^+$-Si and $NiCoO_x$ regions, and the sample was examined by CV and incident photon to current efficiency (IPCE) measurements. The difference between the overpotentials $\eta$ required to obtain a 10 mA $cm^{-2}$ with the $p^+$-Si/Co/$NiCoO_x$ (under dark) and $n^+pp^+$-Si/Co/$NiCoO_x$ (38.6 mW $cm^{-2}$ under the back illumination) reveals a photovoltage ($V_{ph}$) of ~ 510 mV (Figure S3), which is in good agreement with the $V_{ph}$ determined for our previous $p^+pn^+$ Si photocathode with Pt catalyst under same light spectrum condition.[27]

Figure 3 shows spectrally resolved IPCE measurement results of the $n^+pp^+$-Si/Co/$NiCoO_x$ photoanode under back side and front side illumination. Each data point was measured at an applied bias of 1.4 V vs. RHE, at which the sample shows a saturated photocurrent for both front and back side illumination. As shown in Figure 3, the IPCE under the back side illumination increases gradually and shows IPCE close to 85% at 550 nm for photons, which are absorbed near the back side of the sample. Considering the light absorption depth of Si as a function of the wavelength,[27] this high IPCE response is natural since the charge collecting pn-junction is placed at the back side of the sample, and this shows that this $n^+pp^+$-Si/Co/$NiCoO_x$ structure is an efficient configuration to be used as a bottom cell of the tandem device. The low IPCE response in the short wavelength range (~ 500 nm) is mainly attributed to the high recombination rate at the $n^+$-Si surface. Note that we did not apply any surface passivation treatment, and there is no significant optical loss due to the quartz cover glass in this wavelength range.[27] Conversely, the IPCE of the same sample under front side illumination increases slowly from the short wavelength region and reaches merely 30% at a wavelength of 800 nm because most of the electron-hole pairs are generated far from the pn-junction under the front illumination, and due to the poor transmittance of the $NiCoO_x$ layer as shown in Figure 2. Note

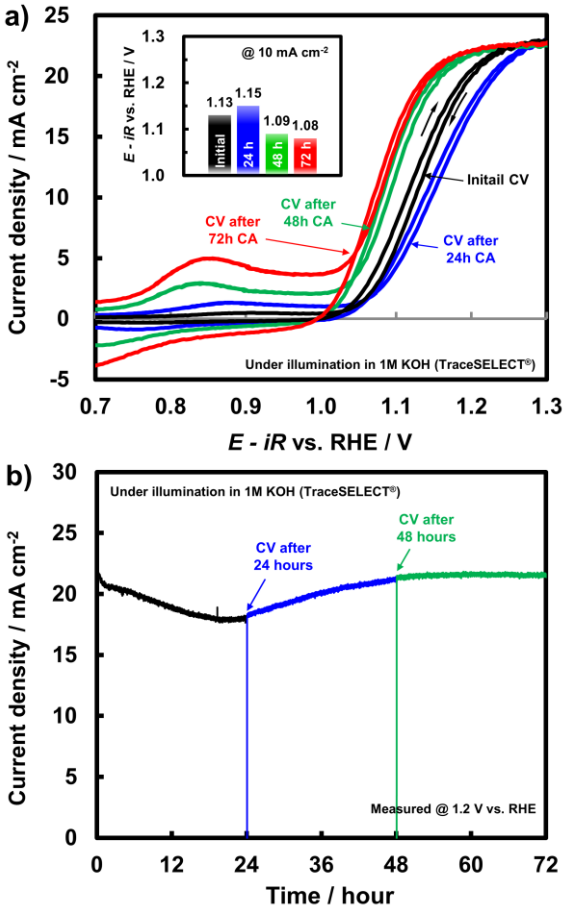


**Figure 4.** (a) Cyclic voltammetry graphs of $n^+pp^+$Si/Co/$NiCoO_x$ photoanode measured before chronoamperometry measurement (black), after the 24 hours long chronoamperometry (blue), after the 48 hours (green), and after the 72 hours long chronoamperometry (red). (b) CA measurements carried out at 1.2 V vs. RHE. The potentials required to achieve a photocurrent density of 10 mA $cm^{-2}$ measured every 24 hours can be found in inset of 4a.

that imperfect active-area definition by epoxy (Loctite 1C Hysol) encased electrodes can cause a overrating of IPCE[32], but not affect on the qualitative behavior. This difference in IPCE behavior between the front and back side illumination is reflected in the CV measurement results (inset in Figure 3). The saturated photocurrent of the $n^+pp^+$-Si/Co/$NiCoO_x$ photoanode sample is around 21 mA $cm^{-2}$ under the back side illumination with approximate AM 1.5G + 635 nm long pass filters, whereas significantly lower photocurrent, less than 5 mA $cm^{-2}$ was measured under front illumination.

In order to investigate time-dependant behavior of the sample, repeated CV measurements with long-term chronoamperometry (CA) measurements were carried out. As shown in Figure 4a, the potential required to achieve a photocurrent density ($J_{ph}$) of 10 mA $cm^{-2}$ was found to depend on the operating time. An applied potential of 1.13 V was required for the initial CV curve. This performance compares well our previous study with an as-deposited NiO, which showed relatively gradual slope, requiring an applied potential of ~ 1.24 V to reach the 10 mA $cm^{-2}$

benchmark[16] This enhanced performance of $NiCoO_x$ is in good agreement with that from the previous electrochemical study on as-deposited Ni-Co-O OER catalyst.[10] Addition of Co, which abounds in the spinel structure of nickel oxide, is known to provide more active sites, and reduce intrinsic electrical resistivity.[9,33] Tseung and Jasem[34] suggested that the mixed valences of the nickel and cobalt cations are helpful in the reversible adsorption of oxygen by providing donor-acceptor sites for chemiabsorption, thus lowering the overpotential. Such synergetic effects are not limited to Ni-Co oxides, for instance recent studies on Ni-Fe-O oxides[13,14] can be understood in the same context. Nevertheless, 1.18 V (at 10 mA $cm^{-2}$) was required for the CV measured after 24 hours chronoamperometry test at 1.2 V, reflecting the changes in OER kinetics. These CV curves (initial and 24h after) showed a similar saturation current $J_{ph}$ (~ 22 mA $cm^{-2}$), but they behaved differently. Compared with the initial CV curve, the curve taken after 24 hours had an anodic shift of 20 mV at 10 mA $cm^{-2}$ and a decreased slope resulting a significant loss at the maximum power point (lower fill factor), which can result in significant loss of operating current density in tandem devices[35] and can be attributed to the $NiCoO_x$ catalyst layer. The anodic shift accompanying with the decreased slop might be explained by the reaction of Co-O compounds with the alkaline electrolyte. Boettcher's group reported in their recent work that ppb-level iron impurities in KOH electrolyte substitute for $Co^{3+}$ under the applied potential, and this substitution incorporation decreases the electrical conductivity of the CoOOH phase,[36] and our ICP-MS analysis revealed Fe of approximately 30 ppb in the electrolyte. In this report, the reduced conductivity appears as a lowered the fill factor (i.e. decreased slope in CV curve). Since our photoanode sample with sputtered $CoO_x$ showed a continuous anodic shift of onset potential with decreased fill factor, this resulted in an increase in overpotential of approximately 40 mV after 3 days operation (Figure S4). This is in agreement with the recent report by the Lewis' group that the $CoO_x$ coupled with a Si photoanode shows a gradual loss in catalytic activity associated with the conversion of $CoO_x$ to $Co(OH)_2$ and then to ion-permeable cobalt oxyhydroxide (CoOOH).[22]

Interestingly, the required bias potential to reach 10 mA $cm^{-2}$ rebounded in the cathodic direction after the first 24 hours and reached 1.07 V vs. RHE after the 3 days of chronoamperometry measurement. Furthermore, the slope of CV curves increased sharply compared to that of the CV curve taken right after the first 24 hours. Since the photoanode with $Co/CoO_x$ showed a continuous anodic shift of onset voltage as well as degradation in photocurrent, it appears reasonable to assume that the increased activity is mainly attributed to the incorporation of $Fe^{3+}$ with $Ni^{2+}$. A number of recent studies[13,14,16] have revealed that the apparent OER activity of NiO is dramatically affected by small amounts of Fe impurities in alkaline electrolyte, causing a cathodic shift in the OER onset potential. The increased redox peak in Figure 4a also implies a strong interaction of Fe with

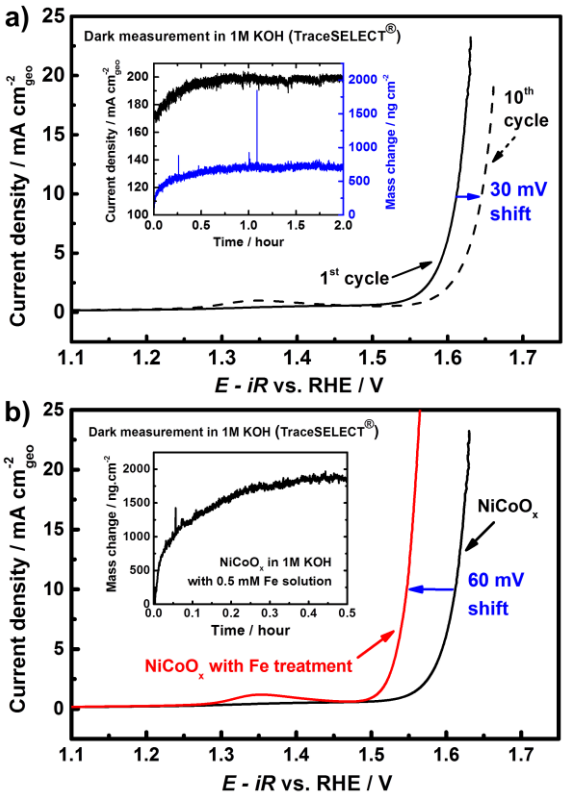


**Figure 5.** (a) Electrochemical cyclic voltammetry measurement result for the $NiCoO_x$ deposited on EQCM sample with Co interlayer with subsequent 2 hours long chronoamperometry and mass change measurement data (inset), and (b) electrochemical current-potential of $NiCoO_x$ before (black) and after Fe-treatment (red). Both chronoamperometry and mass change measurements were carried out with fixed applied potential of 1.8 V vs. RHE using EQCM's.

metal sites, such as Co and/or Ni. The integrated area under the redox feature yields the total charge exchanged between the incorporated ions and the active sites of the electrode,[37] and thus the increased redox features shown in Figure 4a may indicate that a significant number of metallic sites have become electrochemically accessible. The redox wave peak of the oxidative current slightly shifted cathodically for the CV curves taken after 24h and 48h relative to that of the initial CV curve, then anodically shifted toward the OER current peak. The later anodic shift of the redox wave is well known for the binary metal oxides, i.e. $CoO_x$ and NiO. This anodic redox wave shift observed in Figure 4a is consistent with the previous reports,[13,36] where the redox wave for $Co^{2+/3+}$ and $Ni^{2+/3+}$ shifts anodically as the Fe content in the oxide films increases.

However, only few studies reported the presence of the negative shift of redox peak. J. M. Marioli et al.[38] observed that this negative shift takes place for the Ni-Cr binary oxide films, whereas single component nickel oxide showed only anodic redox peak shift. S. Kim et al. also reported[39] that the shifts in the $Ni^{2+/3+}$ redox features in the negative direction (> 50 mV) is induced by the presence of Co in the Ni hydrous oxide lattice. In agreement with the previous observations by other

groups,[10,38,39] no discernible voltammetry features associated with the $Co^{2+/3+}$ redox couple can be identified for the composite Ni-Co oxide film. Despite of a harmony with previous observations, the precise effect on the catalytic mechanism remains unknown.

The CA study performed at 1.2 V versus RHE for 3 days (Figure 4b) reflects the above mentioned behavior of CV curves. At a fixed potential of 1.2 V vs. RHE, the $J_{ph}$ of the $n^+pp^+$-Si/Co/$NiCoO_x$ dropped quite quickly from around 22 to 20.5 mA $cm^{-2}$ over about half an hour, after which photocurrent output appears to degrade slowly with constant rate. This degradation continued during the first 20 hours of CA measurement, followed by a slow increase in $J_{ph}$ after ~ 22 hours followed by a stabilized $J_{ph}$ from the 3rd day of the CA experiment. Once the $J_{ph}$ saturated, the sample showed stable $J_{ph}$ output until 144th hours (6 days) without any further changes or degradation (Figure S5). Assuming that incorporation rate or diffusion rate of Fe thought the ion-permeable oxyhydroxide structures is independent of time, these CV and CA behaviors are interesting. They suggest that Fe incorporation in the beginning is insufficient to lead to increased activity, but sufficient to lead to decreased activity due to the iron incorporated cobalt oxyhydroxide components. Subsequently the Fe incorporation becomes sufficient to cause an improved OER activity after a certain point. It was found that this V-shape of the Si photoanode with Co/$NiCoO_x$ is reproducible, as confined by an additional CA experiment using a new, but similar, sample showed the same time-dependent behavior (see Figure S6).

The electrochemical properties of $NiCoO_x$ thin film deposited on electrochemical quartz crystal microbalance (EQCM) sample were investigated by means of CV and CA in 1 M KOH (TraceSelect) under dark condition (Figure 5). The as-deposited $NiCoO_x$ films (Figure 5, black trace) show quite good performance for the OER. An overpotential of ~ 380 mV is required to achieve a current density of 10 mA $cm^{-2}$ which is in good agreement with the overpotentials obtained in the photoelectrochemical tests (Figure 4a). Nevertheless, after 10 cycles the potential at 10 mA $cm^{-2}$ is shifted anodically by 30 mV. The anodic shift closely resembles the drop in current density in the long-term stability PEC tests and the corresponding anodic shift of the CV curves (Figure 4a). Subsequent 2 hours long CA measurement (Figure 5a inset) showed increase in current density along with mass change during the first 0.5 hours. Afterwards, the $NiCoO_x$ thin film deposited on EQCM was intentionally doped with Fe (Figure 5b, $NiCoO_x$ in KOH with 0.5 mM Fe) according to a procedure previously used for NiO thin films.[16] The EQCM result (Figure 5b inset) shows a significant increase in mass during treatment of NiO in a Fe-containing solution, which was found to be saturated after ~ 0.5 h of treatment. This behavior is similar to mass change for as-deposited $NiCoO_x$ in Figure 5a. We attribute this increase in mass at least partially to Fe incorporation occurring in parallel with oxygen evolution. Interestingly, in the subsequently performed CV measurement (Figure 5b) a cathodic shift of 60 mV compared to the as-prepared $NiCoO_x$ thin film was observed. Thus, an overpotential of ~ 320 mV was required to obtain a current density of 10 mA $cm^{-2}$. This enhanced performance of the Fe-doped $NiCoO_x$ thin film is in good agreement with the enhancement during prolonged CA of the $NiCoO_x$ thin film used for the back-illuminated PEC studies and can therefore be attributed to a self-driven enhancement of nickel cobalt oxide by metallic Fe-contamination during photoelectrochemical oxygen evolution reaction. To further investigate on this, X-ray photoelectron spectroscopy (XPS) was performed. XPS measurements were performed on as-prepared $NiCoO_x$ thin films (prepared on EQCM substrates) and on $NiCoO_x$ thin films after 24h of continuous operation at a potential of 1.8 V vs. RHE. Detailed scans of the Ni 2p and Co 2p regions derived from the survey spectra in Figure 6a are included in Figure 6b and 6c. The as prepared $NiCoO_x$ thin film consists of a mixture of $Ni^{2+}/Ni^{3+}$ (at binding energies of 854/856 eV) and $Co^{2+}/Co^{3+}$ (suggested by the satellite feature at 785 eV). After continuous testing for 24 h XPS measurements reveal that Ni and Co are mainly present in their 3+ oxidation state (binding energy of 856 eV for $Ni^{3+}$ shown in Figure 6b. For $Co^{3+}$ a characteristic binding energy of 780.5 eV was measured. Furthermore, the characteristic $Co^{2+}$ satellite signal at 785 eV was significantly reduced as shown in Figure 6c). The presence of different oxidation states in the as-prepared $NiCoO_x$ thin film as well as its further oxidation during prolonged testing is in good agreement with previously reported NiO thin films prepared and tested under similar conditions[16] and can be ascribed to the transformation into its more porous NiOOH and CoOOH oxidation states which act as hosts for Fe-impurities.[19,36] Binding energy increase of O1s peak (Figure S7) for the tested sample is also support the formation of the oxyhydroxide phase.[40] The direct detection of Fe by means of XPS was not possible in this case due to the Al source's strong overlap with Ni LMM Auger signal and the unfavorable Fe cross section. Using Mg Ka source, which was not available for the XPS used

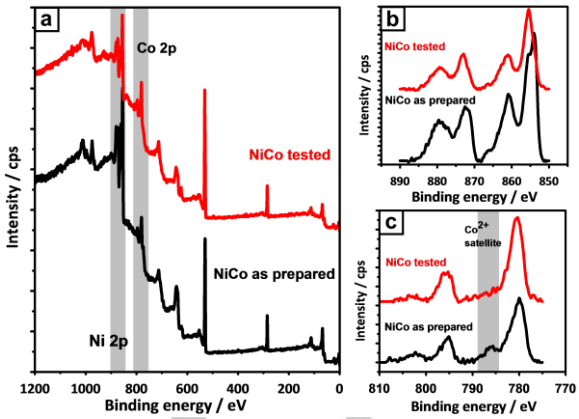


**Figure 6.** (a) XPS survey spectra of the $NiCoO_x$ thin film deposited on EQCM substrate with Co interlayer, and zoomed in (b) Ni 2p XPS spectra, (c) Co 2p region. Black and red color correspond to the curve for the as prepared and after the electrochemical test, respectively.

in this work, would allow detection of trace Fe. However, the transformations into more open NiOOH and CoOOH in the $NiCoO_x$ thin film accompanied with the presented data of $NiCoO_x$ studied on EQCM substrate strongly suggest the self-driven enhancement of nickel cobalt oxide by metallic Fe-contamination during prolonged photoelectrochemical oxygen evolution reaction. In addition, Ni and Fe distribution mapped by EDX (Figure S7) of the porous $NiCoO_x$ deposited on the Si photoanode after 6 days of CA testing at 1.2 V versus RHE also directly supports the presence of Fe, along with above mentioned EQCM results.

## Conclusions

A back-illuminated $n^+pp^+$-Si has been coupled to earth-abundant Ni-Co based catalysts and investigated as photoanode for the oxygen evolution reaction. Specifically we have demonstrated the performance of a $n^+pp^+$-Si/Co/$NiCoO_x$ structure, whose pn-junction is formed at the side opposing the solid/liquid interface, may efficiently drive the OER under back side (dry side) illumination which will be the actual operational condition in a tandem water splitting device. Importantly, taking advantage of the synergetic effects between Ni and Co, the $NiCoO_x$ OER catalyst coating exhibits excellent catalytic activity as well as long-term stability in highly concentrated alkaline media, which makes it a strong candidate for the practical OER catalysts. Interestingly, the photoanode samples activated by $NiCoO_x$ show a non-trivial time-dependent current-voltage behavior in OER activity. In 1M KOH the sample studied initially exhibits an anodic shift of onset potential, followed by a rebound in the cathodic direction which is likely due to Fe incorporation into Ni-Co oxyhydroxide which acts as a host for Fe incorporation. This work highlights an approach to using a low band gap photoanode in actual tandem device operation condition, and enhancing its photocatalytic activity by simple aging process.

## Experimental Section

### Sample fabrication

The shallow $n^+p$-junction was produced in p-type (100) czochralski (CZ) Si wafers (Topsil, 1-20 ohm-cm, boron-doped) by a shallow phosphorous ion implantation at 36 keV with a dose of $3\times10^{15}$ $cm^{-2}$. After annealing a mesa-isolated $n^+p$-Si structure with height of 3 µm is formed at the back side (light illumination side) by photolithography and dry etching (Here, we used Ar, $O_2$ and $CHF_3$ gases in an Oxford Instruments RIE80). The front side of the same samples was also doped with boron doping using ion implantation at 100 keV with a dose of $5\times10^{16}$ $cm^{-2}$ to form a thin $p^+$ layer. An Al charge collecting layer with a circular hole for light irradiation was deposited by e-beam evaporation with a metallic shadow mask to make circular rings for light irradiation. More fabrication details also can be found in our previous work[27] and Supporting Information.

Prior to the deposition of the $NiCoO_x$ protective OER catalyst, the Si was sputtered in Ar to clean the surface and remove the native oxide. Subsequently, a 10 nm Co metallic film was reactively sputtered in 3 mTorr of pure Ar followed by the deposition of 50 nm of $NiCoO_x$ in 3 mTorr at an $O_2$/Ar ratio of 40% by co-sputtering of Ni and Co targets with same deposition rate (i.e. Ni:Co ≈ 1:1). In case of EQCM and glass substrates, Co/$NiCoO_x$ thin films were deposited using the same process conditions as mentioned above. Samples prepared only with cobalt oxide ($Co/CoO_x$) are used to verify qualitatively the role of the Ni component in the binary oxide layer during the reaction. The back side of the samples was covered with a 300 µm thick quartz glass, and was mounted directly onto the Al layer. The resulting active area after covering with epoxy was measured by image analysis using ImageJ 1.46r after the experiments. Schematic cross-sectional configuration and its energy band diagram are shown in Figure 1, and a more detailed description of the related calculation procedure also can be found in Supporting Information.

### Characterization

Photoanodes consisting of $n^+pp^+$Si/Co/$NiCoO_x$ were evaluated under back-side illumination using a 1000 W Xenon lamp (Oriel) with AM 1.5g and 635 nm cut-off filters to appropriately approximate the wavelengths and intensity that this electrode would receive in a practical tandem water splitting device. All CV and chronoamperometry experiments were done in a 3 electrode quartz cell, since intensive corrosion of conventional pyrex can poison or cover the active surface with glass corrosion products,[41] and consequently hinder the light absorption. All (photo) electrochemical measurements were performed in high-purity aqueous 1 M KOH (Aldrich, TraceSELECT®, ≥ 99.995%) using a Bio-Logic VSP potentiostat with EC Lab software. A Pt mesh was used as a counter electrode and the reference was a saturated Hg/HgO electrode (Koslow Scientific Company). The detailed experimental setup and procedure are provided in the Supporting Information. The solution was purged with Ar gas 30 minutes prior to any experiment. Inductively coupled plasma mass spectrometry (ICP–MS) experiments were performed (Thermo Fisher Scientific, iCAP-QC) for the quantification of iron impurity in the electrolyte.

To determine efficiency as a function of wavelength, IPCE measurements were employed. An Oriel 74100 monochromator was combined with the Xenon lamp mentioned above to give monochromatic light. IPCE measurements were carried out from 400 to 800 nm under both front side and back side illumination. To confirm the conductivity type of the present $NiCoO_x$ thin film, electrochemical impedance measurements were performed (Mott-Schottky plot analysis) under the dark condition. Both IPCE and Mott-Schottky analyses were carried out using same equipment and setup as that used for CV measurements.

The results in the present work also cover the electrochemical stability of the $NiCoO_x$ film, and therefore, emphasis also has been put on electrochemical measurements using EQCM samples under the dark conditions to monitor the mass change that occurs during the electrochemical reaction. For this purpose, a three electrode setup similar to that of photocatalytic CV and CA measurements was used. The EQCM measurements were performed with a 5 MHz QCM200 supplied by Stanford Research Systems.

In order to determine the structural properties, XPS analysis was carried out in an UHV (ultra-high vacuum) system provided by Thermo Scientific. In this work, an Al Kα X-ray source emitting photons with energy 1486.7 eV has been used.

SEM with EDX was also carried out for the surface morphology and cross-sectional investigations using Quanta FEG SEM. The provided electron beam energy was 5 to 20 kV with a working distance of around

10 cm. The transmittance spectra were recorded using a Varian Cary 1E UV-Vis Spectrophotometer to estimate band-gap and optical absorption of the deposited Co/$NiCoO_x$ ($NiCoO_x$ on top) and Co/$CoO_x$ layers on quartz substrate. To avoid the effect of background signal, including the absorption by the substrate and/or light scattering particulates in the instrument, a baseline correction using a bare quartz substrate has been carried out prior to the measurements for the $NiCoO_x$ and $CoO_x$ deposited samples.

## Acknowledgements

This work was performed as a part of the Center for Individual Nanoparticle Functionality (CINF) which is funded by Danish National Research Foundation (DNRF54).

**Keywords:** oxygen evolution, nickel cobalt oxide, water splitting, solar fuel, photocatalysis

[1] N. S. Lewis and D. G. Nocera, *Proc. Natl. Acad. Sci. USA* **2006**, *103*, 15729–15735.

[2] B. Laursen, S. Kegnæs, S. Dahl, I. Chorkendorff, *Energy Environ. Sci.* **2012**, *5*, 5577-5591.

[3] S. Dah, I. Chorkendorff, *Nat. Mater.* **2012**, *11*, 100–101.

[4] Y. Lee, J. Suntivich, K. J. May, E. E. Perry, Y. Shao-Horn, *J. Phys. Chem. Lett*. **2012**, *3*, 399–404.

[5] E. A. Paoli, F. Masini, R. Frydendal, D. Deiana, C. Schlaup, M. Malizia, T. W. Hansen, S. Horch, I. E. L. Stephens, I. Chorkendorff, *Chem. Sci.* **2015**, *6*, 190-196.

[6] B. Mei, B. Seger, T. Pedersen, M. Malizia, O. Hansen, I. Chorkendorff, *J. Phys. Chem. Lett*. **2014**, *5*, 1948-1952.

[7] W. Chen, H. Wang, Y. Li, Y. Liu, J. Sun, S. Lee, J.-S. Lee, Y. Cui, *ACS Cent. Sci.* **2015**, *1*, 244-251.

[8] W. T. Hong, M. Risch, K. A. Stoerzinger, A. Grimaud, J. Suntivich, Y. Shao-Horn, *Energy Environ. Sci.* **2015**, *8*, 1404-1427.

[9] H. B. Wu, H. Pang, X. W. Lou, *Energy Environ. Sci.* **2013**, *6*, 3619-3626.

[10] C. Zhu, D. Wen, S. Leubner, M. Oschatz, W. Liu, M. Holzschuh, F. Simon, S. Kaskel, A. Eychmüller, *Chem. Commun.* **2015**, *51*, 7851-7854.

[11] M. Hussain, Z. H. Ibupoto, M. A. Abbasi, X. Liu, O. Nur, M. Willander, *Sensors* **2014**, *14*, 5415-5425.

[12] S. Goodwin-Johansson, P. H. Holloway, G. McGuire, L. Buckley, R. Cozzens, R. Schwarz, G. Exarhos, *Proc. of SPIE* **2000**, *3987*, 225-231.

[13] L. Trotochaud, S. L. Young, J. K. Ranney, S. W. Boettcher, *J. Am. Chem. Soc.* **2014**, *136*, 6744-6753.

[14] D. Friebel, M. W. Louie, M. Bajdich, K. E. Sanwald, Y. Cai, A. M. Wise, M.-J. Cheng, D. Sokaras, T.-C. Weng, R. A. Mori, R. C. Davis, J. R. Bargar, J. K. Nørskov, A. Nilsson, A. T. Bell, *J. Am. Chem. Soc.* **2015**, *137*, 1305-1313.

[15] D. A. Corrigan, R. S. Conell, C. A. Fierro, D. A. Scherson, *J. Phys. Chem.* **1987**, *91*, 5009-5011.

[16] B. Mei, A. A. Permyakova, R. Frydendal, D. Bae, T. Pedersen, P. Malacrida, O. Hansen, I. E. L. Stephens, P. C. K. Vesborg, B. Seger, I. Chorkendorff, *J. Phys. Chem. Lett.* **2014**, *5*, 3456-3461.

[17] J. A. Haber, Y. Cai, S. Jung, C. Xiang, S. Mitrovic, J. Jin, A. T. Bell, J. M. Gregoire, *Energy Environ. Sci.* **2014**, *7*, 682-688.

[18] J. B. Gerken, S. E. Shaner, R. C. Massé, N. J. Porubsky, S. S. Stahl, *Energy Environ. Sci.* **2014**, *7*, 2376-2382.

[19] J. Yang, K. Walczak, E. Anzenberg, F. M. Toma, G. Yuan, J. Beeman, A. Schwartzberg, Y. Lin, M. Hettick, A. Javey, J. W. Ager, J. Yano, H. Frei, I. D. Sharp, *J. Am. Chem. Soc.* **2014**, *136*, 6191-6194.

[20] I. M. Sadiek, A. M. Mohammad, M. E. El-Shakre, M. I. Awad, M. S. El-Deab, B. E. El-Anadouli, *Int. J. Electrochem. Sci.* **2012**, *7*, 3350-3361.

[21] Y. Zhao, S. Chen, B. Sun, D. Su, X. Huang, H. Liu, Y. Yan, K. Sun, G. Wang, *Sci. Rep.* **2015**, *5*, 7629.

[22] X. Zhou, R. Liu, K. Sun, D. Friedrich, M. T. McDowell, F. Yang, S. T. Omelchenko, F. H. Saadi, A. C. Nielander, S. Yalamanchili, K. M. Papadantonakis, B. S. Brunschwig and N. S. Lewis, *Energy Environ. Sci.* **2015**, *8*, 2644-2649.

[23] K.Sun, F. H. Saadi, M. F. Lichterman, W. G. Hale, H.-P. Wang, X. Zhou, N. T. Plymale, S. T. Omelchenko, J.-H. Hee, K. M. Papadantonakis, B. S. Brunschwig, N. S. Lewis, *Proc. Natl. Acad. Sci. USA* **2015**, *12*, 3612-3617.

[24] Y. Yang, H. Fei, G. Ruan, C. Xiang, J. M. Tour, *ACS Nano* **2014**, *8*, 9518-9523.

[25] B. Beverskog, I. Puigdomenech, *Corros. Sci.* **1997**, *39*, 969−980.

[26] E. M. Garcia, J. S. Santos, E. C. Pereira, M. B. J. G. Freitas, *J. Power Sources* **2008**, *185*, 549-553.

[27] D. Bae, T. Pedersen, B. Seger, M. Malizia, A. Kuznetsov, O. Hansen, I. Chorkendorff, P. C. K. Vesborg, *Energy Environ. Sci.*, **2015**, *8*, 650-660.

[28] S. U. Offiah, A. C. Nwanya, S. C. Ezugwu, B. T. Sone, R. U. Osuji, M. Malik, C. D. Lokhande and F. I. Ezema, *Int. J. Electrochem. Sci.* **2014**, *9*, 5837–5848.

[29] K. Deori, S. Deka, *CrystEngComm* **2013**, *15*, 8465-8474.

[30] X. Chen, J. P. Cheng, Q. L. Shou, F. Liu, X. B. Zhang, *CrystEngComm* **2012**, *14*, 1271-1276.

[31] J. F. Marco, J. R. Gancedo, M. Gracia, J. L. Gautier, E. I. Ríos, H. M. Palmer, C. Greaves, F. J. Berry, *J. Mater. Chem.* **2001**, *11*, 3087-3093.

[32] H. Döscher, J. L. Young, J. Geisz, J. Turner, T. Deutsch, *Energy Environ. Sci.* **2016**, Accepted, DOI: 10.1039/C5EE03206G.

[33] G. Wu, N. Li, D.-R. Zhou, K. Mitsuo, B.-Q. Xu, *J. Solid State Chem.* **2004,** *177*, 3682-3692.

[34] P. Rasiyah, A. C. C. Tseung, *J. Electrochem. Soc.* **1983**, *130*, 2384-2386.

[35] H. S. Jeon, J. H. Koh, S. J. Park, M. S. Jee, D.-H. Ko, Y. J. Hwang, B. K. Min, *J. Mater. Chem. A* **2015**, *3*, 5835-5842.

[36] M. S. Burke, M. G. Kast, L. Trotochaud, A. M. Smith, S. W. Boettcher, *J. Am. Chem. Soc.*, **2015**, *137*, 3638−3648.

[37] F. A. Armstrong in *Advances in inorganic chemistry: Iron-sulfur proteins*, *Vol. 38* (Ed. R. Cammack), Academic Press, London, **1992**, p. 125.

[38] D. E. Pissinis, L. E. Sereno, J. M. Marioli, *Open J. Phys. Chem.*, **2012**, *2*, 23-33.

[39] S. Kim, D. A. Tryk, M. R. Antonio, D. Scherson, *Preprint of ACS symposium on recent advances in fuel cells*, *batteries*, **1993** Fall (Chicago) **38** (4), 1457-1463.

[40] M. C. Biesinger, B. P. Payne, L. W. M. Lau, A. Gerson, R. S. C. Smart, *Surf. Interface Anal.* **2009**, *41*, 324-332.

[41] K. J. J. Mayrhofer, G. K. H. Wiberg, M. Arenz, *J. Electrochem. Soc.*, **2008**, *155*, 1-5.

**Entry for the Table of Contents** (Please choose one layout)

Layout 1:

FULL PAPER

**Binary metal oxide under back-illumination**: crystalline Si (c-Si) coupled with a thin layer of $NiCoO_x$ is applied as a photoanode for water oxidation under back-side illumination to be used as a bottom cell of the tandem water splitting device. The thin layer of $NiCoO_x$ effectively protects c-Si from the alkaline electrolyte for 6 days under oxygen evolution reaction.

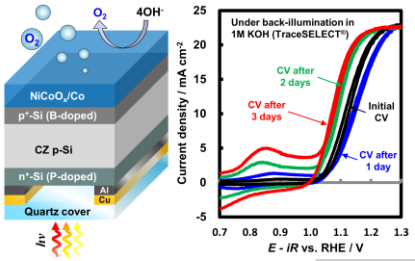


*Dowon Bae, Bastian Mei, Rasmus Fryndendal, Thomas Pedersen, Brian Seger, Ole Hasen, Peter C. K. Vesborg, Ib Chorkendorff**

***Page No. – Page No.***

**Back-illuminated Si based photoanode with nickel cobalt oxide catalytic protection layer**

Layout 2:

FULL PAPER

((Insert TOC Graphic here; max. width: 11.5 cm; max. height: 2.5 cm))

*Author(s), Corresponding Author(s)**

***Page No. – Page No.***

**Title**

Text for Table of Contents